Meteoritics & Planetary Science 36, 1697–1709 (2001)
Available online at http://www.uark.edu/meteor

Radar constraints on asteroid regolith properties using 433 Eros as ground truth

CHRISTOPHER MAGRI[1]*, GUY J. CONSOLMAGNO, S. J.[2,3], STEVEN J. OSTRO[4], LANCE A. M. BENNER[4] AND BRETT R. BEENEY[1]

[1]University of Maine at Farmington, 173 High Street, Preble Hall, Farmington, Maine 04938, USA
[2]Specola Vaticana, V-00120, Vatican City State
[3]Vatican Observatory Research Group, Steward Observatory, University of Arizona, Tucson, Arizona 85721, USA
[4]300-233, Jet Propulsion Laboratory, California Institute of Technology, Pasadena, California 91109-8099, USA
*Correspondence author's e-mail address: magri@maine.edu

(Received 2001 July 12; accepted in revised form 2001 October 30)
(Part of a series on the NEAR–Shoemaker mission to 433 Eros)

Abstract–Radar data enable us to estimate an asteroid's near-surface bulk density, thus providing a joint constraint on near-surface porosity and solid density. We investigate two different approaches to simplifying this joint constraint: estimating solid densities by assuming uniform porosities for all asteroids; and estimating porosities by assuming uniform mineralogy within each taxonomic class. Methods used to estimate asteroids' near-surface solid densities from radar data have not previously been calibrated *via* independent estimates. Recent spacecraft results on the chondritic nature of 433 Eros now permit such a check, and also support porosity estimation for S-class objects.

We use radar albedos and polarization ratios estimated for 36 main-belt asteroids and nine near-Earth asteroids to estimate near-surface solid densities using two methods, one of which is similar to the uncalibrated algorithms used in previous studies, the other of which treats Eros as a calibrator. We also derive porosities for the same sample by assigning solid densities for each taxonomic class in advance. Density-estimation results obtained for Eros itself are consistent with the uncalibrated method being valid in the mean; those derived for the full sample imply that uncalibrated solid densities are, at most, a few tens of percent too large on average. However, some derived densities are extremely low, whereas most porosity estimates are physically plausible. We discuss the relative merits of these two approaches.

INTRODUCTION

Radar experiments provide valuable information on asteroid regoliths by probing the region within several wavelengths (~1 m) of the target's surface. Echoes received in both the same circular polarization sense to that transmitted (SC) and in the opposite circular sense (OC) permit us to estimate the bulk density and degree of decimeter-scale structure within this near-surface region (*e.g.*, Ostro, 1998). (In this paper, "OC" denotes "opposite circular" not "ordinary chondrite".) Each bulk density estimate provides a joint constraint, otherwise difficult to obtain, on porosity and solid density; the latter property in turn depends on metal content and silicate specific gravity, that is, on mineralogy.

There are two extreme methods for simplifying this joint constraint. One method is to assume that all asteroids' near-surface porosity is 50%, which is roughly similar to that of the lunar regolith; this assumption yields an estimate of near-surface solid density. The opposite approach is to fix each asteroid's solid density at a value appropriate for its visible/near-infrared taxonomic class (*i.e.*, at a grain density value measured for the appropriate meteoritic analog); on this assumption the radar data allow us to estimate porosities.

The solid-density-estimation approach was used with main-belt asteroids (MBAs) by Magri *et al.* (1999), but it relies on a very strong simplifying assumption (uniform porosities). The porosity-estimation approach is new, and it assumes mineralogical uniformity only within a given taxon; yet even this weaker assumption is unlikely to be entirely valid. Rather than choosing, we will take both approaches in this work and then will discuss which set of assumptions and results seems more physically plausible.

Recent spacecraft-derived results on the composition of near-Earth asteroid (NEA) 433 Eros are highly relevant to these two methods. X-ray and infrared data obtained during the NEAR–Shoemaker mission indicate that Eros has L- or LL-chondritic composition (*e.g.*, Squyres *et al.*, 2000). Since Eros is also a detected radar target, we can use it as a calibrator for estimating solid densities, by assuming that other asteroids' near-surface layers differ from that of Eros only in Fresnel reflectivity. If, on the other hand, we wish to use radar data to estimate

Prelude preprint MS#4594

© Meteoritical Society, 2001. Printed in USA.

porosities, the new Eros results suggest what solid density we should assume for all S-class targets.

After describing the Eros radar data in "Observations", we will apply each method in turn to our sample of 45 radar-detected MBAs and NEAs, estimating solid densities in "Estimating Near-Surface Solid Densities" and instead estimating porosities in "Estimating Near-Surface Porosities". This sample (see Table 1) consists of 36 MBAs and nine NEAs with reasonably reliable estimates of OC radar albedo; note that there are many other NEAs, which have been detected, but which have poorly constrained projected areas (and hence albedos). In "Solid Densities or Porosities?" we will discuss the strengths and weaknesses of these two extreme approaches.

OBSERVATIONS

Eros was observed at Arecibo during 1988 November 30 to December 5, over which interval the target's average right ascension, declination, and distance from Earth were 23.9 h, +30°, and 0.49 AU, respectively. Dual-polarization 12.6 cm data with raw frequency resolution of 2.84 Hz were obtained for 35 transmit/receive runs; rotation-phase coverage for the experiment was good. Techniques for data acquisition and reduction were nearly identical to those described by Ostro *et al.* (1992). The weighted sum of the 35 Doppler spectra is displayed in Fig. 1. The summed OC spectrum has a signal-to-noise ratio (SNR) of 18 after being optimally filtered in frequency.

We can use this sum to estimate OC cross-section σ_{OC}—the projected area of a perfectly conducting sphere, placed at the target's location, which would produce the OC echo power received from the target—and circular polarization ratio $\mu_C \equiv$ SC/OC. The results are $\sigma_{OC} = 75 \pm 20$ km^2 and $\mu_C = 0.22 \pm 0.06$. The uncertainty on the latter estimate is due largely to receiver noise, while that on σ_{OC} is dominated by systematic calibration uncertainties (~25%). The Arecibo telescope also was used on these dates to observe the Galilean satellites Europa, Ganymede, and Callisto at 12.6 cm, and the resulting cross sections are in close accord with those obtained in other years (Ostro *et al.*, 1992); we conclude that the system was well calibrated in late 1988 and hence that our Eros cross-section estimate is reliable.

In January 1975, Jurgens and Goldstein (1976) used the Goldstone radar system to observe Eros at both 3.5 and 12.6 cm. The corresponding rotation-averaged cross-section estimates are roughly 25 and 38 km^2, one-third to one-half as large as our 1988 value; we attribute this to pointing or calibration errors in the older dataset. In support of this interpretation we note that 12.6 cm Goldstone observations of Ganymede made only 5 months earlier (Goldstein and Morris, 1975) yielded a published cross-section at least 5× smaller than that currently accepted. Note as well that the 3.5 cm μ_{OC} value obtained by Jurgens and Goldstein on one of their four observing dates gave a cross-section 1.8× lower than the mean of the other three dates, a fact which those authors attributed to pointing errors.

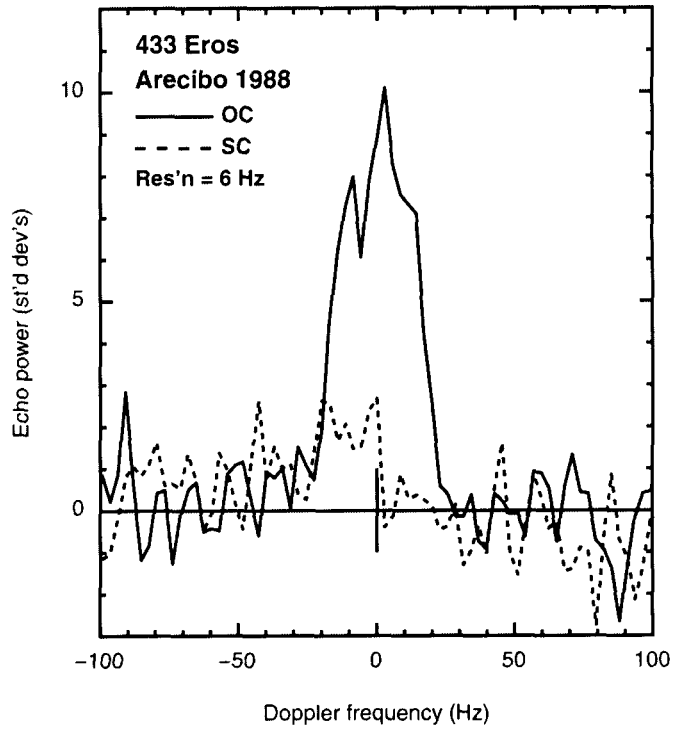

FIG. 1. Weighted sums of opposite circular (OC) (solid line) and SC (dashed line) echo spectra for 433 Eros, smoothed to an effective resolution of 6 Hz. Echo power, in units of standard deviations of the noise, is plotted *vs.* Doppler frequency (Hz) relative to that of hypothetical echoes from the target's center of mass. The vertical bar at the origin indicates ±1 sigma of the OC noise.

Campbell *et al.* (1976) observed Eros from Arecibo at 70 cm in January 1975; the higher of their two cross-section estimates is 39 ± 15 km^2, compatible with those of Jurgens and Goldstein but only half of our 1988 value. We have no explanation for this discrepancy with the 1988 data, noting only that any pointing errors in 1975 would reduce the cross-section.

Based on the established reliability of the system during the 1988 experiment (see above), we weight that cross-section estimate twice as strongly as the 38 km^2 estimate from 1975. Thus we use $\sigma_{OC} = 63 \pm 20$ km^2 as our best estimate of Eros' OC cross-section.

The 3.5 cm experiment of Jurgens and Goldstein yielded $\mu_C = 0.33^{+0.08}_{-0.05}$ based on the ratio of σ_{SC} and σ_{OC} each averaged over a full rotation, and roughly 0.37 based on the ratio of the maximum cross sections observed in time-resolved data. The corresponding figures for the (weaker) 12.6 cm data are 0.22 ± 0.15 and 0.38 ± 0.19, respectively. The unweighted mean of these four estimates is 0.33. Since systematic errors largely cancel out of the polarization ratio, we give this mean value equal weight with the 1988 result, obtaining $\mu_C = 0.28 \pm 0.06$ as our best estimate.

If we know a target's mean projected area $\langle A_{proj} \rangle$ over the duration of a radar experiment, we can estimate the OC radar albedo $\hat{\sigma}_{OC} \equiv \sigma_{OC}/\langle A_{proj} \rangle$. The spacecraft-derived shape

TABLE 1. Radar data and solid density estimates.[†]

Name	Class	NEA	μ_C	$\hat{\sigma}_{OC}$	Ref.	d_{solid} (uncalibrated)			d_{solid} (Eros-calibrated)		
41 Daphne	C		0.13 ± 0.08	0.11 ± 0.03	1	3.4	+1.1,	−0.9	2.4	+0.7,	−0.5
78 Diana	C		0.00 ± 0.08	0.13 ± 0.03	1	4.4	+1.3,	−1.0	2.7	+0.8,	−0.5
105 Artemis	C		0.15 ± 0.04	0.16 ± 0.06	1	4.0	+1.4,	−1.2	3.0	+0.9,	−0.8
144 Vibilia	C		0.18 ± 0.10	0.11 ± 0.03	1	3.2	+1.1,	−1.1	2.4	+0.7,	−0.5
194 Prokne	C		0.16 ± 0.04	0.23 ± 0.07	1	4.8	+1.6,	−1.3	3.6	+1.1,	−0.9
356 Liguria	C		0.12 ± 0.06	0.13 ± 0.04	1	3.8	+1.2,	−1.0	2.7	+0.8,	−0.6
654 Zelinda	C		0.13 ± 0.03	0.18 ± 0.05	1	4.4	+1.4,	−1.1	3.2	+0.9,	−0.7
2100 Ra-Shalom	C	*	0.31 ± 0.02	0.16 +0.17, −0.09	2	2.9	+1.7,	−2.1	3.0	+1.5,	−1.2
1 Ceres	G		0.03 ± 0.03	0.041 ± 0.003	1	2.3	+0.6,	−0.4	1.5	+0.4,	−0.2
2 Pallas	B		0.05 ± 0.02	0.076 ± 0.007	1	3.1	+0.8,	−0.6	2.0	+0.5,	−0.3
19 Fortuna	G		0.06 ± 0.04	0.076 ± 0.024	1	3.1	+1.0,	−0.8	2.0	+0.6,	−0.5
46 Hestia	P		0.00 ± 0.11	0.074 ± 0.018	1	3.3	+0.9,	−0.8	2.0	+0.6,	−0.4
84 Klio	G		0.23 ± 0.06	0.15 ± 0.06	1	3.4	+1.2,	−1.4	2.9	+0.9,	−0.8
139 Juewa	CP		0.10 ± 0.10	0.061 ± 0.022	1	2.6	+0.9,	−0.8	1.8	+0.5,	−0.5
324 Bamberga	CP		0.15 ± 0.04	0.066 ± 0.008	1	2.5	+0.7,	−0.6	1.9	+0.5,	−0.3
554 Peraga	FC		0.06 ± 0.06	0.22 ± 0.07	1	5.5	+1.8,	−1.4	3.5	+1.1,	−0.9
694 Ekard	CP:		0.00 ± 0.10	0.09 ± 0.03	1	3.6	+1.1,	−1.0	2.2	+0.7,	−0.5
5 Astraea	S		0.20 ± 0.03	0.20 ± 0.04	1	4.2	+1.3,	−1.1	3.3	+0.9,	−0.6
6 Hebe	S		0.00 ± 0.12	0.16 ± 0.03	1	4.9	+1.4,	−1.2	3.0	+0.8,	−0.6
7 Iris	S		0.18 ± 0.10	0.11 ± 0.02	1	3.2	+1.0,	−1.0	2.4	+0.7,	−0.4
8 Flora	S		0.16 ± 0.05	0.10 ± 0.02	1	3.1	+0.9,	−0.8	2.3	+0.6,	−0.4
9 Metis	S		0.14 ± 0.04	0.13 ± 0.03	1	3.7	+1.1,	−0.9	2.7	+0.8,	−0.5
12 Victoria	S		0.14 ± 0.03	0.22 ± 0.04	1	4.9	+1.4,	−1.1	3.5	+1.0,	−0.6
18 Melpomene	S		0.30 ± 0.10	0.16 ± 0.04	1	3.0	+1.2,	−2.1	3.0	+0.9,	−0.6
20 Massalia	S		0.28 ± 0.07	0.16 ± 0.05	1	3.2	+1.2,	−1.6	3.0	+0.9,	−0.7
27 Euterpe	S		0.34 ± 0.08	0.10 ± 0.05	1	2.1	+1.0,	−2.1	2.3	+0.8,	−0.8
33 Polyhymnia	S		0.07 ± 0.11	0.14 ± 0.06	1	4.2	+1.5,	−1.5	2.8	+0.9,	−0.8
80 Sappho	S		0.25 ± 0.05	0.14 ± 0.05	1	3.2	+1.1,	−1.3	2.8	+0.9,	−0.7
192 Nausikaa	S		0.00 ± 0.11	0.13 ± 0.04	1	4.4	+1.4,	−1.2	2.7	+0.8,	−0.6
230 Athamantis	S		0.00 ± 0.12	0.22 ± 0.08	1	5.9	+2.0,	−1.8	3.5	+1.1,	−0.9
433 Eros	S	*	0.28 ± 0.06	0.25 ± 0.09	3	4.0	+1.5,	−2.0	3.8	+0.1,	−0.1
532 Herculina	S		0.37 ± 0.15	0.09 ± 0.05	1	1.8	+1.2,	−1.8	2.2	+0.8,	−0.9
3199 Nefertiti	S	*	0.47 ± 0.04	0.32 +0.19, −0.10	4	1.6	+2.2,	−1.6	4.3	+1.7,	−1.1
4179 Toutatis	S	*	0.29 ± 0.01	0.21 ± 0.03	5	3.6	+1.1,	−1.4	3.4	+1.0,	−0.6
4769 Castalia	S	*	0.31 ± 0.02	0.16 ± 0.03	5	3.0	+1.0,	−1.4	3.0	+0.8,	−0.6
6489 Golevka	S	*	0.23 ± 0.02	0.18 ± 0.09	5	3.8	+1.5,	−1.6	3.2	+1.1,	−1.1
16 Psyche	M		0.17 ± 0.05	0.31 ± 0.06	1	5.6	+1.7,	−1.5	4.2	+1.2,	−0.8
21 Lutetia	M		0.22 ± 0.07	0.17 ± 0.06	1	3.7	+1.3,	−1.4	3.1	+0.9,	−0.8
97 Klotho	M		0.23 ± 0.07	0.21 ± 0.05	1	4.1	+1.4,	−1.4	3.4	+1.0,	−0.7
216 Kleopatra	M		0.00 ± 0.05	0.6 ± 0.1	6	11.3	+3.5,	−2.5	6.1	+2.0,	−1.2
796 Sarita	M		–	0.25 ± 0.08	1		–		3.8	+1.2,	−0.9
6178 1986 DA	M	*	0.09 ± 0.02	0.58 ± 0.09	7	9.5	+2.8,	−2.0	5.9	+1.9,	−1.1
4 Vesta	V		0.28 ± 0.05	0.12 ± 0.04	1	2.7	+1.0,	−1.3	2.6	+0.8,	−0.6
1862 Apollo	Q	*	0.33 ± 0.01	0.12 ± 0.07	4	2.4	+1.1,	−2.4	2.6	+0.9,	−1.0
2063 Bacchus	QSV	*	0.21 ± 0.01	0.33 +0.25, −0.11	8	5.4	+2.8,	−1.7	4.3	+2.0,	−1.1

[†]The first two columns list the target name and taxonomic class. An asterisk in the third column indicates a near-Earth asteroid. The next two columns give circular polarization ratio $\mu_C \equiv$ SC/OC and OC radar albedo $\hat{\sigma}_{OC}$, taken from the sources listed in the sixth column and references therein: (1) Magri *et al.* (1999); (2) Shepard *et al.* (2000); (3) this paper; (4) Ostro *et al.* (1991a,b); (5) Ostro *et al.* (2001); (6) Ostro *et al.* (2000); (7) Ostro *et al.* (1991a); (8) Benner *et al.* (1999). Albedo uncertainties have been set to a minimum of 15% to account for inter-target calibration uncertainties, except for 324 Bamberga for which interferometric data also exist. No SC data are available for 796 Sarita. The seventh column gives near-surface solid density as estimated using the method of Magri *et al.* (1999); the eighth lists the same quantity estimated using 433 Eros as a calibrator (see text). All tabulated uncertainties are standard errors.

model for Eros has projected areas 331, 320, and 150 km^2 when viewed along the short, intermediate, and long principal axes, respectively (P. Thomas, pers. comm.). In order to estimate $\langle A_{\text{proj}} \rangle$ we treat Eros as a triaxial ellipsoid whose axis lengths are $2a \geq 2b \geq 2c$ and which has the projected areas listed above; this yields $2a$ = 30.0 km, $2b$ = 14.1 km, and $2c$ = 13.6 km. A triaxial ellipsoid viewed over a full rotation has mean projected area

$$\langle A_{\text{proj}} \rangle = \pi ab \times \frac{2}{\pi} E(k) \sqrt{\sin^2 \delta + \left(\frac{c}{b}\right)^2 \cos^2 \delta} \qquad (1)$$

Here δ is the subradar latitude, and $E(k)$ is the complete elliptic integral of the second kind,

$$E(k) = \int_0^{\pi/2} \sqrt{1 - k^2 \sin^2 \theta}\, d\theta \qquad (2)$$

whose modulus k is given by

$$k = \sqrt{\frac{1 - \left(\frac{b}{a}\right)^2}{\left(\frac{b}{c}\right)^2 \tan^2 \delta + 1}} \qquad (3)$$

The spacecraft-derived pole direction (Veverka *et al.*, 2000) implies that during the 1988 radar experiment the average subradar latitude was δ = 17°. Inserting this value and the axis lengths listed earlier into Eqs. (1–3) yields mean projected area 253 km^2, and so we adopt the estimate $\langle A_{\text{proj}} \rangle$ = 250 ± 30 km^2. The small uncertainty reflects the quality of the rotation phase coverage: our data cover a wide range of viewing geometries, so our *mean* projected area cannot be close to the minimum (end-on) value of 150 km^2 or to the maximum (broadside) value ~320 km^2.

Dividing the OC cross-section by this area gives OC albedo $\hat{\sigma}_{\text{OC}}$ = 0.25 ± 0.09. The error on this estimate is dominated by the cross-section uncertainty.

ESTIMATING NEAR-SURFACE SOLID DENSITIES

Methods

Uncalibrated Method–Dual circular-polarization asteroid experiments yield estimates of OC cross-section σ_{OC}, circular polarization ratio μ_{C}, and (if mean projected area $\langle A_{\text{proj}} \rangle$ is known) OC radar albedo $\hat{\sigma}_{\text{OC}}$. SC cross-section σ_{SC} and SC radar albedo $\hat{\sigma}_{\text{SC}}$ are defined analogously to their OC counterparts. An OC-only echo (μ_{C} = 0) represents "quasispecular" reflection: single backscattering from surface elements that are smooth at decimeter scales. For targets with nonzero σ_{SC}, some of the echo power is instead due to "diffuse" scattering, that is, to single scattering from rough surfaces, irregularly shaped rocks, or other structures, and/or to multiple scattering. If the diffuse echo is characterized by OC albedo $\hat{\sigma}_{\text{OC, diff}}$ and by polarization ratio $\mu_{\text{C,diff}} \equiv \hat{\sigma}_{\text{SC}} / \hat{\sigma}_{\text{OC, diff}}$, then we can write

$$\hat{\sigma}_{\text{OC, diff}} = \frac{\hat{\sigma}_{\text{SC}}}{\mu_{\text{C, diff}}} = \frac{\mu_{\text{C}} \hat{\sigma}_{\text{OC}}}{\mu_{\text{C, diff}}} \qquad (4)$$

so the component of the target's OC albedo due to quasispecular reflection is

$$\hat{\sigma}_{\text{OC, qs}} = \hat{\sigma}_{\text{OC}} - \hat{\sigma}_{\text{OC, diff}} = \hat{\sigma}_{\text{OC}} \left(1 - \frac{\mu_{\text{C}}}{\mu_{\text{C, diff}}}\right) \qquad (5)$$

We adopt $\mu_{\text{C, diff}}$ = 0.50 ± 0.15; the 2 sigma interval 0.20–0.80 covers most measured values tabulated by Harmon and Ostro (1985) for the Moon and inner planets.

We next use radar albedo(s) to estimate the Fresnel reflectivity R. A smooth, spherical target would produce a specular echo characterized by $\hat{\sigma}_{\text{OC}} = R$ and $\hat{\sigma}_{\text{SC}} = 0$. If we instead consider a target which is entirely covered with large, smooth, tilted surface facets, we must modify this simple relation, at the same time taking care not to employ a model too complex to be constrained by the available data. For example, the simple quasispecular scattering law of Hagfors (1964) often provides a good empirical fit to planetary radar data despite its being based on an unphysical assumption about the scattering surface (Simpson and Tyler, 1982).

Further modification is needed if there is wavelength-scale structure in (and hence diffuse scattering from) the near-surface layers. A proper treatment of diffuse scattering would involve detailed numerical simulations for individual rocks of various shapes, sizes, and burial depths, such as was explored by Baron *et al.* (1997, 1998)—but our limited asteroid radar data could not possibly support such a detailed model. Evans and Hagfors (1966) handle diffuse scattering by writing a simple expression for the total radar albedo $\hat{\sigma}_{\text{total}} \equiv \hat{\sigma}_{\text{OC}} + \hat{\sigma}_{\text{SC}}$:

$$\hat{\sigma}_{\text{total}} = gR \qquad (6)$$

where g is the backscatter gain, varying from unity for a perfectly smooth sphere to 3 or higher for a rock-covered target. In this spirit, we follow Magri *et al.* (1999) and work with the quasispecular albedo alone (Eq. (5)):

$$\hat{\sigma}_{\text{OC, qs}} = gR \qquad (7)$$

An anonymous reviewer argues that we underestimate our quasispecular albedo (and hence, by Eq. (7), underestimate R) because we normalize it to the full geometric area $\langle A_{\text{proj}} \rangle$ rather

than to that fraction of the area, which contributes to quasispecular reflection. Empirically, we will see in "Comparison of Two Density-Estimation Methods and Compositional Inferences" that densities obtained *via* the "uncalibrated" algorithm currently being described may be several tens of percent too large; it follows that increasing these estimates by 10 to 20% (by normalizing $\hat{\sigma}_{OC,qs}$ to a smaller projected area) would be a step in the wrong direction. We lack any independent constraints on what the fractional rock coverage might be for any of our asteroid targets, and it is also the case that there are substantial uncertainties on most targets' geometric projected areas even prior to correction.

On the theoretical side, there is no literature consensus on how to treat the diffuse-scattering component. Even for the simple case of a two-component (smooth *vs.* rocky) surface model, Hagfors and Evans (1968) equate the reflectivities of the two components but assume a much higher gain for the rocky component than for the smooth one, whereas Ostro *et al.* (1999) equate the two gains but allow rocks to have higher reflectivity than the smooth surface (resulting from higher bulk density; see Eq. (9) below). We also note that these two studies involved the Moon and NEA 4179 Toutatis, respectively, two targets with very high SNR and correspondingly detailed information derivable; by contrast, some of the MBAs in the present dataset have SNR as low as 6.

For all of these reasons we will not attempt to correct our first-order diffuse scattering correction by accounting for fractional rock coverage. This omission becomes noteworthy for asteroids dominated by diffuse echoes, that is, for those with large polarization ratios. Such targets would have uncertain $\hat{\sigma}_{OC,qs}$ values in any event, since the parenthetical correction factor in Eq. (5) becomes small and uncertain. Fortunately, almost all of the asteroids in our sample have small or moderate μ_C values.

The backscatter gain to be used in Eq. (7) is of order $1 + s_0^2/2$ for a spherical target whose surface facets have adirectional root-mean-square (r.m.s.) slope s_0; hence we would not expect g to exceed unity by more than a few tens of percent for real targets viewed over a full rotation (*e.g.*, Mitchell *et al.*, 1996). Let us take g to be 1.2 ± 0.1, corresponding to r.m.s. slope angle ~30° (2 sigma interval 0°–50°).

Once we have used Eq. (7) to estimate R, near-surface bulk density d_{bulk} can be inferred using the empirical relationship presented by Garvin *et al.* (1985) for dry, unconsolidated powders with porosity greater than ~20%:

$$d_{bulk} = \left(3.2\ \mathrm{g\ cm^{-3}}\right) \ln\left(\frac{1+\sqrt{R}}{1-\sqrt{R}}\right) \tag{8}$$

which inverts to

$$R = \tanh^2\left(\frac{d_{bulk}}{6.4\ \mathrm{g\ cm^{-3}}}\right) \tag{9}$$

Equation (8) agrees well with other empirically derived formulae (*e.g.*, Ostro *et al.*, 1985) and should be valid in the mean to within 10% for asteroid surfaces whose reduced metal content is well under 50% (*e.g.*, chondritic material). Powdered metal behaves similarly to powdered rock in the microwave regime, but solid rock containing large metallic inclusions does not (Campbell and Ulrichs, 1969); hence we probably can apply Eq. (8) to 216 Kleopatra, an MBA blanketed with nickel-iron powder (Ostro *et al.*, 2000), but must be wary in applying it to 6178 1986 DA, a metallic NEA which may be too small to have retained fine impact debris (Ostro *et al.*, 1991a).

With d_{bulk} in hand, we use an assumed near-surface porosity p to estimate near-surface solid density d_{solid}:

$$d_{bulk} = (1-p)d_{solid} \tag{10}$$

We assume $p = 0.5 \pm 0.1$, roughly corresponding to the upper 30 cm of the lunar regolith (Heiken *et al.*, 1991; Table 9.5). Hence we can use Eqs. (5), (7), (8), and (10) and our assumed values of g and p to produce solid density estimates from disc-integrated radar data:

$$d_{solid} = \left(\frac{3.2\ \mathrm{g\ cm^{-3}}}{1-p}\right) \ln\left[\frac{1+\sqrt{\frac{\hat{\sigma}_{OC}}{g}\left(1-\frac{\mu_C}{\mu_{C,diff}}\right)}}{1-\sqrt{\frac{\hat{\sigma}_{OC}}{g}\left(1-\frac{\mu_C}{\mu_{C,diff}}\right)}}\right] \tag{11}$$

Eros-Calibrated Method–Magri *et al.* (1999) have used the uncalibrated method outlined in the preceding section to support *relative* density comparisons between MBAs of different taxonomic classes, but it has not previously been demonstrated that these density estimates are correct in an absolute sense. The recent determination of Eros' chondritic composition provides the first independent check on this method: we can use Eros as a calibrator by assuming that other asteroids' near-surface layers differ from that of Eros only in Fresnel reflectivity. The fact that Eros' circular polarization ratio falls within the ±1 sigma interval for our sample implies that this target has a typical degree of near-surface decimeter-scale structure (see "Uncalibrated Method") and hence gives us confidence that our assumptions are a reasonable first approximation.

For the "Eros-calibrated" estimation method we suppose that Fresnel reflectivity and OC radar albedo are related by

$$R = f\hat{\sigma}_{OC} \tag{12}$$

where f is a proportionality constant which is the *same* for all asteroids. Our philosophy here is that of Occam's razor: just as with the uncalibrated method in the preceding section, we analyze our modest SNR data by hypothesizing a very simple relationship between radar albedo and reflectivity.

To obtain f, we assume that Eros is made of L-chondritic material. The mean solid (grain) density for L chondrites is 3.48 ± 0.10 g cm^{-3} (Consolmagno and Britt, 1998; see also Flynn *et al.*, 1999), but Consolmagno *et al.* (1998) argue that terrestrial weathering has lowered the measured grain density of most meteorites in our collections by altering metallic iron into lower-density iron oxides which fill pore spaces. They conclude that one should use not the mean grain density but the highest measured grain density as representative of the pre-weathered state; for L chondrites this maximum value is 3.75 g cm^{-3}. We adopt the estimate $d_{\text{L-CH}} = 3.75 \pm 0.10$ g cm^{-3} and treat this as Eros' near-surface solid density.

If we further assume that all asteroids obey the Garvin *et al.* (1985) laboratory relationship between Fresnel reflectivity and bulk density (Eqs. (8–9)), and that all asteroids have the *same* near-surface porosity p (Eq. (10)), we can derive an expression for f. Applying Eqs. (9–10) to Eros yields

$$R_{\text{Eros}} = \tanh^2\left[\frac{(1-p)d_{\text{L-CH}}}{6.4 \text{ g cm}^{-3}}\right] \tag{13}$$

and hence Eq. (12) gives us

$$f = \frac{R_{\text{Eros}}}{\hat{\sigma}_{\text{OC, Eros}}} = \left(\frac{1}{\hat{\sigma}_{\text{OC, Eros}}}\right)\tanh^2\left[\frac{(1-p)d_{\text{L-CH}}}{6.4 \text{ g cm}^{-3}}\right] \tag{14}$$

It is now possible to obtain an "Eros-calibrated" expression for the near-surface solid densities of all other asteroids. We use the value of f from Eq. (14) in Eq. (12), insert the resulting reflectivity into Eq. (8) to get bulk density; and finally apply Eq. (10) to obtain

$$d_{\text{solid}} = \frac{3.2 \text{ g cm}^{-3}}{1-p} \times \ln\left(\frac{1+\left(\frac{\hat{\sigma}_{\text{OC}}}{\hat{\sigma}_{\text{OC, Eros}}}\right)^{1/2}\tanh\left[\frac{(1-p)d_{\text{L-CH}}}{6.4 \text{ g cm}^{-3}}\right]}{1-\left(\frac{\hat{\sigma}_{\text{OC}}}{\hat{\sigma}_{\text{OC, Eros}}}\right)^{1/2}\tanh\left[\frac{(1-p)d_{\text{L-CH}}}{6.4 \text{ g cm}^{-3}}\right]}\right) \tag{15}$$

As with the uncalibrated method, we assume $p = 0.5 \pm 0.1$. The argument of the tanh function in Eq. (15) is significantly less than unity for realistic porosities, so a series of first-order Taylor expansions can be used to show that d_{solid} is approximately given by

$$d_{\text{solid}} \approx \left(\frac{\hat{\sigma}_{\text{OC}}}{\hat{\sigma}_{\text{OC, Eros}}}\right)^{1/2} d_{\text{L-CH}} \tag{16}$$

that is, approximately (a) independent of the value guessed for near-surface porosity and (b) directly proportional to the assumed value of L-chondrite grain density. The latter result means that treating Eros as an LL chondrite (*i.e.*, as slightly less dense than an L chondrite) would slightly lower our d_{solid} estimates.

Solid Density Results

Linear Approximation to Uncalibrated Method–The uncalibrated method of solid density estimation ("Uncalibrated Method") involves nonlinear relationships, but Fig. 2a shows that a linear fit of d_{solid} as a function of $\hat{\sigma}_{\text{OC}}$ works well. The slope is positive because dense surfaces have high Fresnel reflectivities and hence produce strong quasispecular OC echoes. Rough targets produce a larger fraction of their OC power *via* diffuse scattering and a smaller fraction *via* quasispecular reflection (see Eq. (5)); it follows that for a given value of $\hat{\sigma}_{\text{OC}}$, asteroids with larger μ_{C} produce weaker quasispecular echoes. These targets must have smaller Fresnel reflectivities according to our simple scattering model (see Eq. (7)) and hence must have smaller d_{solid}. Therefore Fig. 2b shows that taking μ_{C} into account yields a better fit.

The discrepant low-density point in Fig. 2a and 2b is 3199 Nefertiti, whose high μ_{C} value (0.47 ± 0.04) implies a rough surface. The uncalibrated estimate for such a target depends sensitively on the assumed value of $\mu_{\text{C, diff}}$ (Eq. (5)). The value used here (0.50 ± 0.15) implies that scattering by Nefertiti is almost entirely diffuse, and hence that the surface has low density. Yet the discrepancy seen in Fig. 2b may mean that this asteroid's surface produces randomly polarized diffuse echo ($\mu_{\text{C, diff}} = 1.0$; see Shepard *et al.*, 2000) and so is denser than derived here. Another possibility is that the OC albedo estimate ($0.32^{+0.19}_{-0.10}$) is significantly low because Nefertiti's diameter estimate, obtained using disc-integrated radiometric data rather than more detailed shape information (see note to Table 1), is significantly high.

Unweighted multiple linear regression of solid density on OC albedo and polarization ratio, using the OC albedos, polarization ratios, and uncalibrated density estimates in Table 1, yields the result

$$d_{\text{solid}} = (13.0 \pm 1.1)\hat{\sigma}_{\text{OC}} - (7.0 \pm 1.3)\mu_{\text{C}} + (2.8 \pm 0.3) \tag{17}$$

The uncertainties listed in Eq. (17) are two or more times larger than the formal standard errors, large enough to span the changes in slope and intercept estimates if we omit Nefertiti from the sample (see discussion above). The regression explains 94% of the variance in the data, and the standard error on density predictions made using this fit (relative to those made using the exact, nonlinear relationships) is 0.43 g cm^{-3}.

Equation (17) holds for porosity $p = 0.5$; to use any other value, multiply the right side of the equation by $0.5/(1 - p)$. Thus we can rewrite the expression as

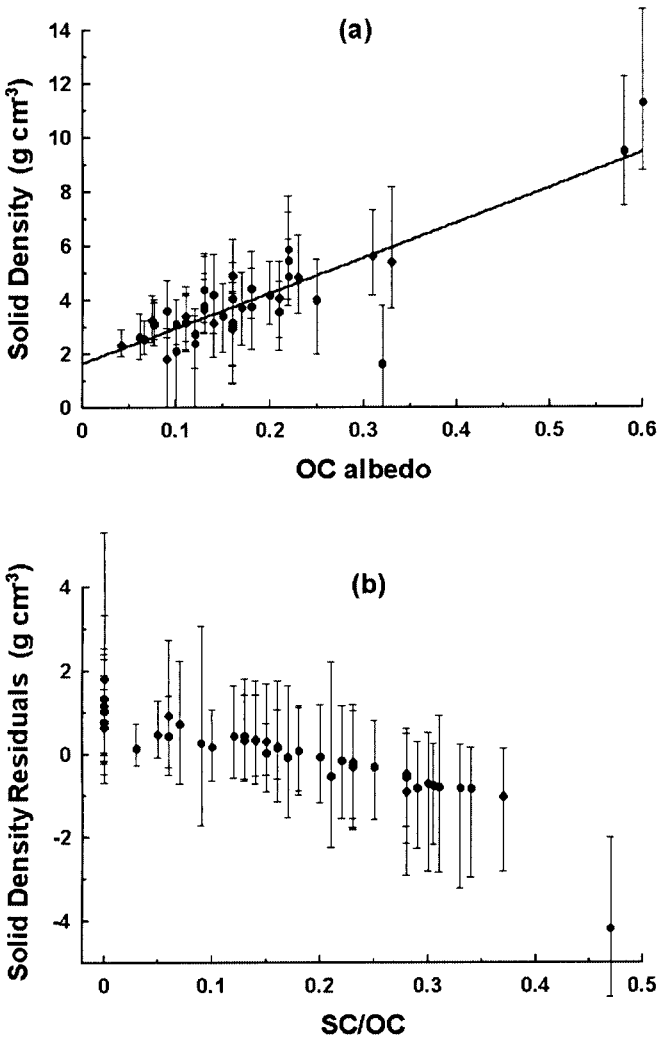

FIG. 2. Near-surface solid densities estimated using the uncalibrated method, shown as functions of opposite circular (OC) albedo and circular polarization ratio. Horizontal error bars have been omitted for clarity. (a) Unweighted linear fit as a function of OC albedo alone. (b) Residuals of the fit shown in (a) plotted against circular polarization ratio.

$$d_{\text{solid}} = \frac{6.5\hat{\sigma}_{\text{OC}} - 3.5\mu_{\text{C}} + 1.41 \pm 0.22}{1-p}\ \text{g cm}^{-3}\ ;\ p > 0.2 \quad (18)$$

We stress that Eq. (18) represents a quick, approximate method of computing solid densities, and that one can always use the full nonlinear relationship (Eq. 11) for higher precision. Note that the uncertainty term in Eq. (18), although chosen to be conservative, may still be underestimated insofar as not all asteroids have the same porosity.

Comparison of Two Density-Estimation Methods and Compositional Inferences–Table 1 lists the radar parameters and the two estimates of d_{solid} for each asteroid in our radar-detected sample, ordered by taxonomic class. We have grouped the nine carbonaceous objects not in the C taxon—the B, FC, G, P, and CP-class targets—into a "BFGP" class. Near-surface solid densities are displayed in Fig. 3 against a backdrop of shaded horizontal bands representing grain density ranges for ordinary and carbonaceous chondrites, for stony-iron meteorites, and for iron meteorites.

A glance at the upper right portion of Fig. 3 reveals that the uncalibrated method yields impossibly high densities for Kleopatra and 1986 DA, two M-class targets with high radar albedos. The best estimates of d_{solid} are only 1 to 1.5σ above the density range of iron meteorites, so this discrepancy may be a statistical fluke. Alternatively, the high estimates may result from inappropriately applying Eq. (8) to metal-rich objects (see "Uncalibrated Method").

The uncalibrated method predicts a d_{solid} value for Eros which is 1.1 ± 0.5× larger than that of L chondrites, a ratio which is statistically consistent with unity. Therefore uncalibrated estimates are correct in the mean. We can make a similar comparison for the entire radar-detected sample, improving the statistics at the expense of requiring additional assumptions (*i.e.*, that the other targets are indeed similar to Eros in the ways outlined in "Eros-Calibrated Method"). The uncalibrated estimates are 1.30× higher in the mean than those obtained using Eros as a calibrator. This mean ratio has a standard error of 0.04 and hence is greater than one at a high significance level. The inter-target variation in this ratio is almost entirely due to variation in μ_{C}: the uncalibrated method makes use of polarization ratio estimates while the Eros-calibrated method does not. More specifically, the uncalibrated-to-calibrated ratio is strongly anticorrelated with polarization ratio. Two or more calibrators will be needed before we can check how (or whether) to adjust density estimates for different μ_{C} values—that is, before we know how or whether f depends on μ_{C}. Meanwhile, we conclude that the uncalibrated estimates are, at most, a few tens of percent too high on average.

Having determined that the two methods yield similar results, we now can inspect Fig. 3 to make compositional inferences for the various taxonomic classes. Solid densities derived for C-class targets are consistent with carbonaceous chondritic composition, as was previously determined for MBAs by Magri *et al.* (1999). The Eros-calibrated estimates imply similarity to the hydrated CI and CM meteorite subtypes, whose grain densities range from 2.2 to 2.9 g cm^{-3} (Britt and Consolmagno, 2000); the uncalibrated estimates tend to be higher, suggesting instead a link with the anhydrous CO and CV subtypes (3.1 to 3.9 g cm^{-3}).

M-class asteroids display a wide range of solid densities, consistent with the conclusion of Magri *et al.* that some (such as Kleopatra) are largely metallic while others (such as 21 Lutetia) are largely rock. Note that Rivkin *et al.* (2000) have detected the 3 μm water-of-hydration feature for Lutetia but not for the higher-albedo objects Kleopatra and 16 Psyche, again consistent with the idea that Lutetia is rocky while the other

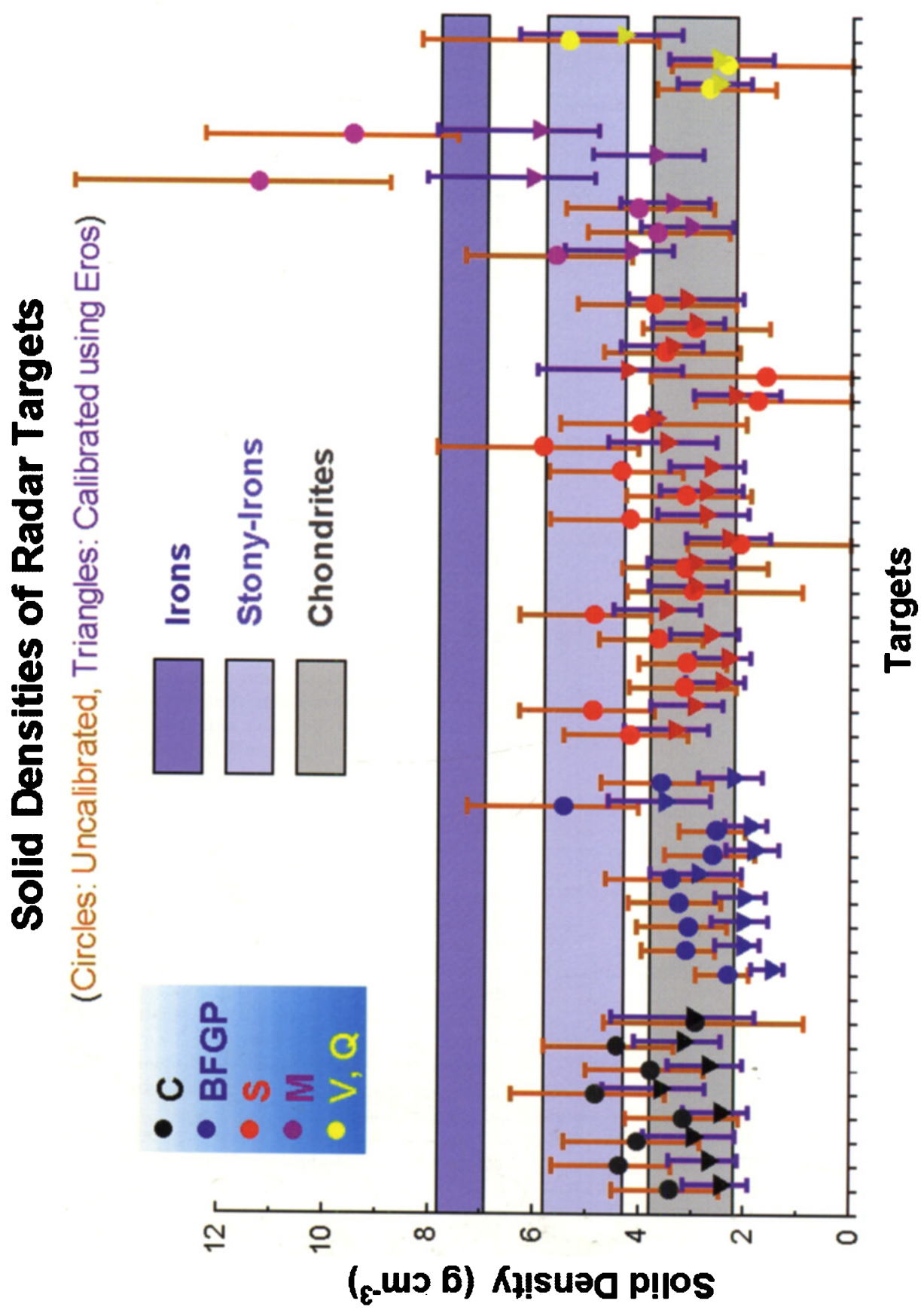

FIG. 3. Near-surface solid densities estimated for radar-detected asteroids using two different methods. Objects have been grouped by taxonomic class, displayed from left to right in the order given in Table 1. Each asteroid has two different density estimates shown, except for 796 Sarita for which no uncalibrated density estimate is possible. Error bars represent standard errors. The lower, middle, and upper shaded bands represent the grain density ranges for chondrites, stony-iron meteorites, and iron meteorites, respectively.

two are metallic. Most of the BFGP-class targets have low densities; in particular, those obtained *via* the Eros-calibrated method are lower than the density of CI chondrites, possibly implying ultraprimitive composition, or else possibly indicating the limitations of our method (see "Solid Densities or Porosities?"). Most radar-detected S-class asteroids are likely to have ordinary chondritic composition, although a minority group of stony-iron analogs cannot be ruled out.

ESTIMATING NEAR-SURFACE POROSITIES

Introduction

How can we estimate near-surface porosities from radar data? Our model makes the same assumptions as does the uncalibrated solid density estimation method ("Uncalibrated Method") except that we treat solid density as known and porosity as unknown. As a result we quickly obtain a rearranged version of Eq. (11):

$$p = 1 - \left(\frac{3.2\ \mathrm{g\ cm^{-3}}}{d_{\mathrm{solid}}}\right) \ln\left[\frac{1+\sqrt{\frac{\hat{\sigma}_{\mathrm{OC}}}{g}\left(1-\frac{\mu_{\mathrm{C}}}{\mu_{\mathrm{C,diff}}}\right)}}{1-\sqrt{\frac{\hat{\sigma}_{\mathrm{OC}}}{g}\left(1-\frac{\mu_{\mathrm{C}}}{\mu_{\mathrm{C,diff}}}\right)}}\right] \quad (19)$$

As with solid density estimation we assume backscatter gain $g = 1.2 \pm 0.1$ and polarization ratio for diffusely scattered radiation $\mu_{\mathrm{C,\,diff}} = 0.50 \pm 0.15$.

We choose d_{solid} values as a function of taxonomic class based on the grain densities of meteoritic analogs, keeping in mind the weathering-based bias toward low measured grain densities ("Eros-Calibrated Method"). Our adopted solid densities are 3.75 g cm^{-3} for S, Q, and QSV objects and 3.3 g cm^{-3} for V. We choose 3.5 g cm^{-3} for C and BFGP, although some of these carbonaceous asteroids are likely to be hydrated (especially the G-class objects) and hence may have lower solid densities (Britt and Consolmagno, 2000). The M taxon is even more difficult to handle, given the large compositional difference between hydrated and unhydrated members (see "Comparison of Two Density-Estimation Methods and Compositional Inferences"). We assume 3.7 g cm^{-3} for Lutetia (appropriate for enstatite chondritic composition) and 7.5 g cm^{-3} for all other M-class asteroids in our sample. The higher density makes sense for Psyche and Kleopatra, which are known to be unhydrated, and is quite plausible for the high-$\hat{\sigma}_{\mathrm{OC}}$ NEA 1986 DA, but it is a guess for the moderate-$\hat{\sigma}_{\mathrm{OC}}$ MBA 97 Klotho.

Given the possibility that our sample includes a few high-density stony-iron S-class targets, low-density hydrated G-class objects, and so on, we conservatively adopt standard errors of 10% on all assumed solid densities. This choice has very little effect on our porosity estimates, whose uncertainties are dominated by the errors on OC albedos and polarization ratios.

Porosity Results

The near-surface porosity estimates for our radar-detected asteroids are listed in Table 2 and displayed in Fig. 4. It is important to emphasize that these values and the densities listed in Table 1 were derived using conflicting physical assumptions about asteroid surfaces: one must choose between the two sets of estimates, because *they cannot both be correct.*

The mean porosity for our sample is 0.51 and the standard deviation is 0.14: most objects have moderate porosities, with only four estimates below 0.30 and only four above 0.70. One of the high estimates, for Klotho, may result from its being incorrectly assigned a metallic solid density; treating it instead as an enstatite chondrite analog (as was done for Lutetia) would lower the porosity to 0.45. However, the low mass reported for Psyche by Viateau (2000) implies that this object, if metallic, has a *volume-averaged* porosity of 0.76 ± 0.09, so it is possible that Klotho is metallic and that some metallic asteroids have extremely porous interiors and near-surface layers. Nefertiti's high porosity may reflect the complications discussed for this object in "Linear Approximation to Uncalibrated Method". At the other extreme, Kleopatra's low porosity estimate is difficult to reconcile with the finding of Ostro *et al.* (2000) that this dog bone-shaped object is blanketed with powdered metal. As was mentioned in "Comparison of Two Density-Estimation Methods and Compositional Inferences", this may indicate a problem with applying Eq. (8) to a metallic target. But we stress that *most* of the porosity estimates are physically plausible.

Visual inspection of Fig. 4 does not indicate any obvious differences between taxonomic classes. We can check this more rigorously by using Levene's test to look for inter-class differences in the spread (variance) of porosity values, and the Kruskal–Wallis test to check for differences in the median porosity (see Magri *et al.*, 1999 and references therein). Neither of these tests reveals any significant differences between classes.

We also used linear regression analysis to see if porosity depends on target diameter, rotation period, visual albedo, (U-B) color, or (B-V) color. (Obviously the (V-I) color would be more interesting to analyze than (U-B) or (B-V): the I filter covers the 1 μm absorption band of olivine and pyroxene, and the strength of this band can depend on the regolith particle size distribution or on the space weathering history (*e.g.*, Binzel *et al.*, 1996). Unfortunately, (V-I) values have not been published for most of our targets.) None of these analyses yielded significant correlations. The strongest correlation, a trend for porosity to increase slightly with increasing visual albedo, was only significant at the 7% level—that is, there is a 7% chance that the asteroid population as a whole does not follow such a trend.

TABLE 2. Porosity estimates.†

Name	Class	NEA	p		
41 Daphne	C		0.51	+0.12,	−0.11
78 Diana	C		0.37	+0.12,	−0.11
105 Artemis	C		0.42	+0.16,	−0.14
144 Vibilia	C		0.55	+0.14,	−0.11
194 Prokne	C		0.31	+0.17,	−0.15
356 Liguria	C		0.46	+0.13,	−0.12
654 Zelinda	C		0.37	+0.13,	−0.13
2100 Ra-Shalom	C	*	0.58	+0.29,	−0.22
1 Ceres	G		0.67	+0.04,	−0.04
2 Pallas	B		0.55	+0.05,	−0.06
19 Fortuna	G		0.56	+0.09,	−0.09
46 Hestia	P		0.54	+0.10,	−0.08
84 Klio	G		0.51	+0.19,	−0.13
139 Juewa	CP		0.63	+0.11,	−0.09
324 Bamberga	CP		0.64	+0.06,	−0.06
554 Peraga	FC		0.22	+0.18,	−0.18
694 Ekard	CP:		0.49	+0.13,	−0.11
5 Astraea	S		0.44	+0.13,	−0.11
6 Hebe	S		0.35	+0.13,	−0.11
7 Iris	S		0.58	+0.12,	−0.09
8 Flora	S		0.59	+0.09,	−0.08
9 Metis	S		0.51	+0.10,	−0.09
12 Victoria	S		0.35	+0.12,	−0.11
18 Melpomene	S		0.60	+0.28,	−0.13
20 Massalia	S		0.58	+0.21,	−0.12
27 Euterpe	S		0.72	+0.28,	−0.11
33 Polyhymnia	S		0.44	+0.18,	−0.15
80 Sappho	S		0.58	+0.16,	−0.11
192 Nausikaa	S		0.42	+0.14,	−0.12
230 Athamantis	S		0.22	+0.22,	−0.19
433 Eros	S	*	0.47	+0.26,	−0.16
532 Herculina	S		0.76	+0.24,	−0.14
3199 Nefertiti	S	*	0.78	+0.22,	−0.28
4179 Toutatis	S	*	0.53	+0.19,	−0.10
4769 Castalia	S	*	0.60	+0.19,	−0.10
6489 Golevka	S	*	0.50	+0.20,	−0.15
16 Psyche	M		0.63	+0.08,	−0.07
21 Lutetia	M		0.50	+0.18,	−0.13
97 Klotho	M		0.73	+0.09,	−0.06
216 Kleopatra	M		0.25	+0.14,	−0.15
796 Sarita	M			–	
6178 1986 DA	M	*	0.37	+0.10,	−0.12
4 Vesta	V		0.59	+0.19,	−0.11
1862 Apollo	Q	*	0.68	+0.32,	−0.12
2063 Bacchus	QSV	*	0.28	+0.21,	−0.28

†The first two columns list the target name and taxonomic class. An asterisk in the third column indicates a near-Earth asteroid. The fourth column gives near-surface porosity estimates and standard errors on those estimates.

SOLID DENSITIES OR POROSITIES?

If we consider only rocky asteroids by ignoring M-class objects, the uncalibrated near-surface solid density estimates in Table 1 range from 1.6 to 5.9 g cm^{-3}, while the Eros-calibrated estimates cover the range 1.5 to 4.3 g cm^{-3}. The uncalibrated values are tied to a uniform near-surface porosity of 0.5; the Eros-calibrated densities are insensitive to the porosity value but still rely on the assumption of *uniform* porosity among asteroids. How physically plausible are these results?

The lower end of these solid density ranges provides cause for concern. There are few minerals on Earth, and none in meteorites, that have a grain density as low as 1.5 g cm^{-3}, and no whole meteorite in our collection comes close to this value. Even interplanetary dust particles, most of which have low bulk densities due to their highly porous structures, are made of materials whose solid densities are chondritic or higher (Grün, 1998). There is no independent empirical evidence supporting our lowest asteroid solid density estimates.

From a theoretical standpoint, rocky material containing roughly cosmic abundances of iron, silicon, magnesium, aluminum, and calcium will have a grain density of around 3.5 to 4.0 g cm^{-3}. A low-metal rock derived from the mantle of a differentiated parent body will have d_{solid} ~3.0 g cm^{-3}; hydrating such material could further lower the density to perhaps 2.5 g cm^{-3} but probably not much lower. Hence the low densities estimated here for some BFGP, C, and (especially) Q and S-class objects seem mineralogically unlikely.

If we instead suppose that we know what asteroid surfaces are made from, based on their visible/near-infrared spectra, then we can compute solid densities rather than attempting to measure them. This in turn allows us to use radar data to estimate porosities. We have employed this philosophy in "Estimating Near-Surface Porosities", yielding the porosity estimates listed in Table 2; as was already noted, most of these estimates seem physically reasonable.

Our density-estimation and porosity-estimation algorithms rest on different sets of assumptions, and while neither set is likely to be uniformly valid—recall that neither method yielded a very satisfactory result for the metal-rich asteroid Kleopatra—we can ask which of these two extreme simplifications (see "Introduction") is more valid in the mean. Which set of mutually exclusive results, the solid densities in Table 1 or the porosities in Table 2, should one trust? Most importantly, now that the Arecibo telescope has been upgraded and new asteroid radar detections are being obtained at an unprecedented rate, which algorithm should we apply in the future to this rapidly increasing dataset?

Porosity estimation has clear advantages over density estimation, as the latter procedure relies on the strong assumption of uniform porosity. We might expect p to vary within a mineralogically uniform set of asteroids, as a result of varying histories (impacts, space weathering) and varying ability to retain fine impact debris (diameter, rotation period).

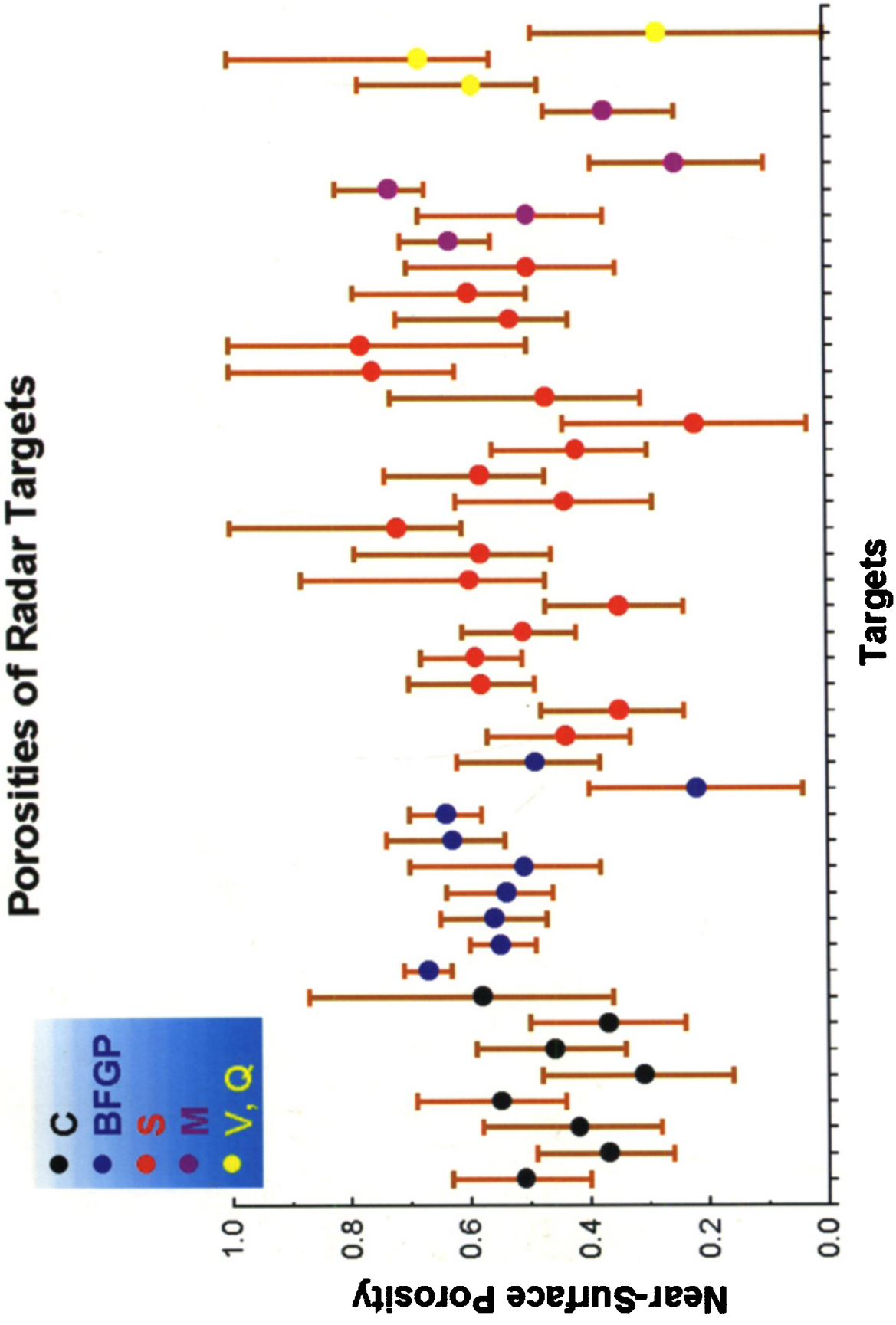

FIG. 4. Near-surface porosities estimated for radar-detected asteroids. Objects have been grouped by taxonomic class, displayed from left to right in the order given in Table 2. Error bars represent standard errors.

Currently there is no empirical evidence against such variation—there are essentially no data at all on asteroidal near-surface porosities. In fact a skeptic could argue that if our set of porosity estimates is more credible overall than is our set of solid density estimates, this merely reflects our greater ignorance as to what constitutes credible porosities. Yet even keeping this caveat in mind, it seems more reasonable to suppose, for example, that the uppermost layers of S-class target 27 Euterpe are highly porous ($p = 0.72$) than that they contain extremely low-density material ($d_{solid} = 2.1$ g cm^{-3}).

Why, then, should we even consider estimating solid densities? Our answer is that the key assumption of the porosity-estimation method—uniform mineralogy within each taxonomic class—prevents us from considering the important issue of intraclass compositional diversity. Does the S taxon include stony-iron analogs in addition to chondritic objects like Eros? What fraction of M-class asteroids are "wet" (hydrated) *vs.* "dry" (anhydrous) objects, and is there some easily obtained discriminant (such as visual albedo; see Magri *et al.*, 1999) between the two? These are important current questions which can be partially addressed using radar data.

One can imagine, though, that the day eventually will come when these questions will have been answered. Once we have obtained and analyzed enough spectral data over a wide enough wavelength range for asteroids covering a wide enough diameter and semimajor-axis range, we will understand how taxonomy relates to composition; we will know how to correct for particle-size and space weathering effects; in short, we will know the solid density of each new radar target before we ever transmit a microwave beam towards it. But it is much harder to imagine that anything short of spacecraft missions involving landers and/or sample return will provide us with independent information about asteroids' near-surface porosities, or that such missions will visit more than a few objects per decade. We conclude that radar-based solid density estimation has its place for now, but that radar-based porosity determination, calibrated *via* spacecraft, is the wave of the future.

Acknowledgments–The Arecibo Observatory is part of the National Astronomy and Ionosphere Center, which is operated by Cornell University under a cooperative agreement with the National Science Foundation and with support from the National Aeronautics and Space Administration (NASA). Part of this research was conducted at the Jet Propulsion Laboratory, California Institute of Technology, under contract with NASA. C. M. was partially supported by NSF grant AST-9973216. B. R. B. was supported through the University of Maine at Farmington Student Work Initiative program.

Editorial handling: B. E. Clark

REFERENCES

BARON J. E., SIMPSON R. A. AND TYLER G. L. (1997) Radiowave scattering from surface rocks: Application to Mars Viking and Pathfinder landing sites (abstract). *Lunar Planet. Sci.* **28**, 69.

BARON J. E., SIMPSON R. A., TYLER G. L., MOORE H. J. AND HARMON J. K. (1998) Estimation of Mars radar backscatter from measured surface rock populations. *J. Geophys. Res.* **103**, 22 695–22 712.

BENNER L. A. M. *ET AL.* (1999) Radar observations of asteroid 2063 Bacchus. *Icarus* **139**, 309–327.

BINZEL R. P., BUS S. J., BURBINE T. H. AND SUNSHINE J. M. (1996) Spectral properties of near-earth asteroids: Evidence for sources of ordinary chondrite meteorites. *Science* **273**, 946–948.

BRITT D. T. AND CONSOLMAGNO G. J. (2000) The porosity of dark meteorites and the structure of low-albedo asteroids. *Icarus* **146**, 213–219.

CAMPBELL D. B., PETTENGILL G. H. AND SHAPIRO I. I. (1976) 70-cm radar observations of 433 Eros. *Icarus* **28**, 17–20.

CAMPBELL M. J. AND ULRICHS J. (1969) Electrical properties of rocks and their significance for lunar radar observations. *J. Geophys. Res.* **74**, 5867–5881.

CONSOLMAGNO G. J. AND BRITT D. T. (1998) The density and porosity of meteorites from the Vatican collection. *Meteorit. Planet. Sci.* **33**, 1231–1241.

CONSOLMAGNO G. J., BRITT D. T. AND STOLL C. P. (1998) The porosities of ordinary chondrites: Models and interpretations. *Meteorit. Planet. Sci.* **33**, 1221–1229.

EVANS J. V. AND HAGFORS T. (1966) Study of radio echoes from the Moon at 23 centimeters wavelength. *J. Geophys. Res.* **71**, 4871–4889.

FLYNN G. J., MOORE L. B. AND KLÖCK W. (1999) Density and porosity of stone meteorites: Implications for the density, porosity, cratering, and collisional disruption of asteroids. *Icarus* **142**, 97–105.

GARVIN J. B., HEAD J. W., PETTENGILL G. H. AND ZISK S. H. (1985) Venus global radar reflectivity and correlations with elevation. *J. Geophys. Res.* **90**, 6859–6871.

GOLDSTEIN R. M. AND MORRIS G. A. (1975) Ganymede: Observations by radar. *Science* **188**, 1211–1212.

GRÜN E. (1998) Interplanetary dust and the zodiacal cloud. In *The Encyclopedia of the Solar System* (eds. P. R. Weissman, L. A. McFadden and T. V. Johnson), pp. 673–696. Academic Press, San Diego, California, USA.

HAGFORS T. (1964) Backscattering from an undulating surface with applications to radar returns from the Moon. *J. Geophys. Res.* **69**, 3779–3784.

HAGFORS T. AND EVANS J. V. (1968) Radar studies of the Moon. In *Radar Astronomy* (eds. J. V. Evans and T. Hagfors), pp. 219–273. McGraw-Hill, New York, New York, USA.

HARMON J. K. AND OSTRO S. J. (1985) Mars: Dual-polarization radar observations with extended coverage. *Icarus* **62**, 110–128.

HEIKEN G. H., VANIMAN D. T. AND FRENCH B. M. (1991) *Lunar Sourcebook.* Cambridge Univ. Press, New York, New York, USA. 736 pp.

JURGENS R. F. AND GOLDSTEIN R. M. (1976) Radar observations at 3.5 and 12.6 cm wavelength of asteroid 433 Eros. *Icarus* **28**, 1–15.

MAGRI C. *ET AL.* (1999) Mainbelt asteroids: Results of Arecibo and Goldstone radar observations of 37 objects during 1980–1995. *Icarus* **140**, 379–407.

MITCHELL D. L. *ET AL.* (1996) Radar observations of asteroids 1 Ceres, 2 Pallas, and 4 Vesta. *Icarus* **124**, 113–133.

OSTRO S. J. (1998) Planetary radar. In *The Encyclopedia of the Solar System* (eds. P. R. Weissman, L. A. McFadden and T. V. Johnson), pp. 773–807. Academic Press, San Diego, California, USA.

OSTRO S. J., CAMPBELL D. B. AND SHAPIRO I. I. (1985) Mainbelt asteroids: Dual-polarization radar observations. *Science* **229**, 442–446.

OSTRO S. J., CAMPBELL D. B., CHANDLER J. F., HINE A. A., HUDSON R. S., ROSEMA K. D. AND SHAPIRO I. I. (1991a) Asteroid 1986 DA: Radar evidence for a metallic composition. *Science* **252**, 1399–1404.

OSTRO S. J. *ET AL.* (1991b) Asteroid radar astrometry. *Astron. J.* **102**, 1490–1502.

OSTRO S. J. *ET AL.* (1992) Europa, Ganymede, and Callisto: New radar results from Arecibo and Goldstone. *J. Geophys. Res.* **97**, 18 227–18 244.

OSTRO S. J. *ET AL.* (1999) Asteroid 4179 Toutatis: 1996 radar observations. *Icarus* **137**, 122–139.

OSTRO S. J., HUDSON R. S., NOLAN M. C., MARGOT J-L., SCHEERES D. J., CAMPBELL D. B., MAGRI C., GIORGINI J. D. AND YEOMANS D. K. (2000) Radar observations of asteroid 216 Kleopatra. *Science* **288**, 836–839.

OSTRO S. J., NOLAN M. C., MARGOT J-L., MAGRI C., HARRIS A. W. AND GIORGINI J. D. (2001) Radar observations of asteroid 288 Glauke. *Icarus* **152**, 201–204.

RIVKIN A. S., HOWELL E. S., LEBOFSKY L. A., CLARK B. E. AND BRITT D. T. (2000) The nature of M-class asteroids from 3 μm observations. *Icarus* **145**, 351–368.

SHEPARD M. K., BENNER L. A. M., OSTRO S. J., HARRIS A. W., ROSEMA K. D., SHAPIRO I. I., CHANDLER J. F. AND CAMPBELL D. B. (2000) Radar observations of asteroid 2100 Ra-Shalom. *Icarus* **147**, 520–529.

SIMPSON R. A. AND TYLER G. L. (1982) Radar scattering laws for the lunar surface. *IEEE Trans. Antennas Propag.* **AP-30,** 438–449.

SQUYRES S. W. *ET AL.* (2000) X-ray and gamma ray spectroscopy at 433 Eros (abstract). *Bull. Am. Astron. Soc.* **32**, 994.

VEVERKA J. *ET AL.* (2000) NEAR at Eros: Imaging and spectral results. *Science* **289**, 2088–2097.

VIATEAU B. (2000) Mass and density of asteroids (16) Psyche and (121) Hermione. *Astron. Astrophys.* **354**, 725–731.